

Molecular simulations for dynamic nuclear polarization in liquids: A case study of TEMPOL in acetone and DMSO

Supporting Information

Sami Emre Küçük,^a Petr Neugebauer,^b Thomas F. Prisner,^b and Deniz Sezer^{a*}

^aFaculty of Engineering and Natural Sciences, Sabancı University, Orhanlı-Tuzla, 34956 Istanbul, Turkey

^bInstitute of Physical and Theoretical Chemistry, Goethe University,

Max-von-Laue Str. 7, 60438, Frankfurt am Main, Germany

(Dated: January 17, 2015)

I. ADDITIONAL RESULTS

A. Analysis of 1 M TEMPOL solutions

The TEMPOL-TEMPOL radial distribution functions (RDFs) calculated from the 1 M TEMPOL simulations are shown in Fig. S1. While the TEMPOL molecules are seen to be well dispersed in acetone and DMSO*, a very small tendency of the radicals to stay closer to each other is seen in the simulation with DMSO.

The near-near (NN) and near-far (NF) contributions to the TEMPOL-solvent dipolar time correlation functions (TCFs) from the 1 M TEMPOL simulations are shown in Fig. S2. The corresponding spectral density functions (SDFs) obtained by Fourier transforming the TCFs are shown in Fig. S3, where the solid lines are analytical fits with the finite-size version^{1,2} of the hard-spheres centered-spins (HSCS) model.^{3,4}

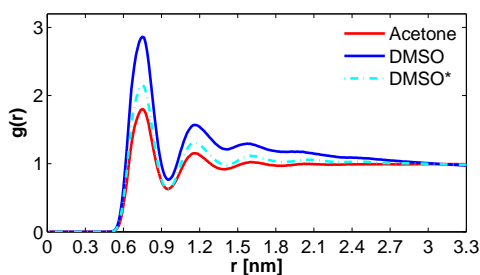


FIG. S1. RDFs between the centers of mass of the TEMPOL molecules in the 1M simulations at 35°C.

The total dipolar SDF and its spatial decomposition are plotted against frequency in Fig. S4.

B. T_1 measurements

Nuclear T_1 values measured for various TEMPOL concentrations, C , are given in Table S1. From these numbers, the relaxivities are calculated as

$$r(C) = \frac{1}{C} \left[\frac{1}{T_1(C)} - \frac{1}{T_1(0)} \right] \quad (\text{S1})$$

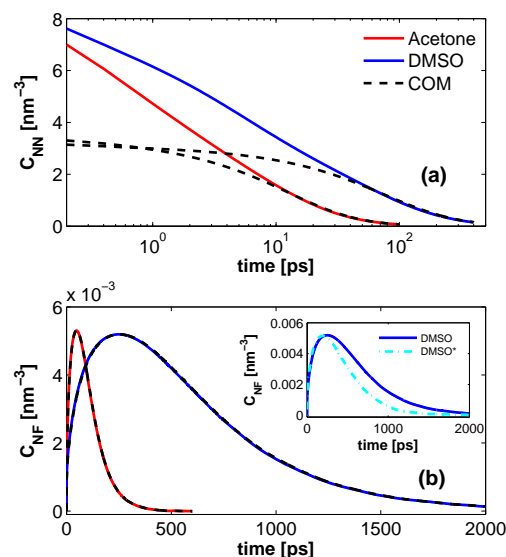


FIG. S2. (a) Near-near and (b) near-far dipolar time correlation functions from the simulations with 1M TEMPOL. Line colors and inset as Fig. 8 of main text.

and reported in Fig. 11 of the main text. In equation (2) of the main text we used the notation $T_1^0 = T_1(0)$ and $T_1^{\text{rad}} = T_1(C)$.

II. METHODS

A. MD simulations

The simulation parameters for acetone and DMSO were from the CHARMM General Force Field (CGenFF),⁶ which uses the literature model of DMSO.⁷ The atomic partial charges of the modified DMSO model, which we called DMSO*, were taken from Ref. 8. The TEMPOL parameters are from Ref. 9.

All MD simulations were performed with NAMD,¹⁰ accounting for electrostatic interactions with the particle-mesh Ewald method.¹¹ In all simulations the temperature was kept at 35°C with a Langevin thermostat. Cubic boxes with periodic boundary conditions were used. An

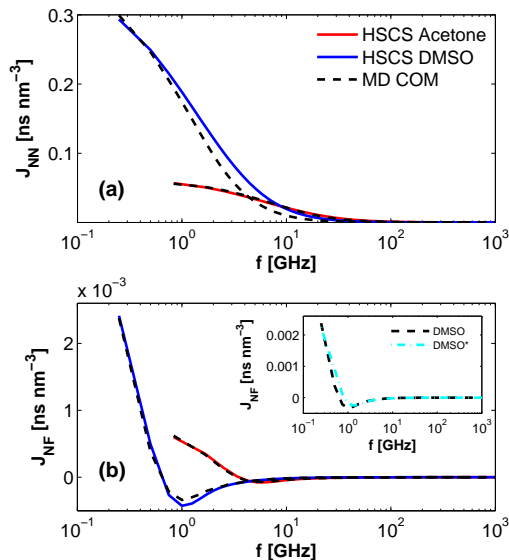


FIG. S3. (a) Near-near and (b) near-far dipolar spectral density functions from the simulations with 1M TEMPOL. Line colors and inset as Fig. 9 of main text.

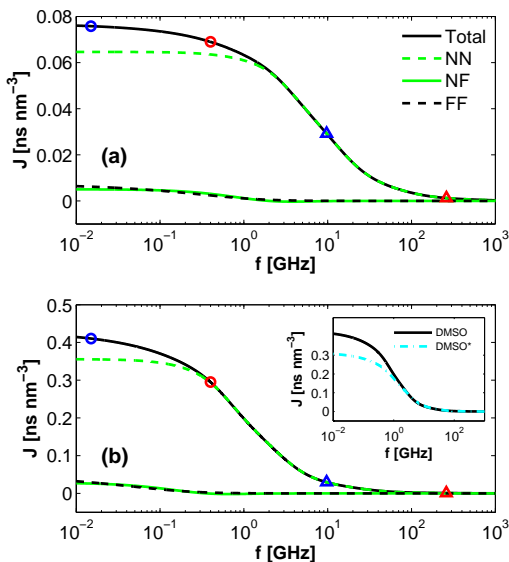


FIG. S4. Dipolar SDF and its additive contributions from the simulations with 1 M TEMPOL in acetone (a) and DMSO (b). Symbols indicate SDF values at proton (o) and electron (Δ) Larmor frequencies at 0.33 T (blue) and 9.2 T (red). The inset of (b) compares the SDFs of DMSO and DMSO*.

integration time step of 2 fs was employed in conjunction with SETTLE.¹²

First, cubic boxes containing 2744 solvent molecules were created. For each solvent, the size of the simulation box, L , was selected to match the experimental densities of acetone and DMSO at 35°C (Table S2). By care-

TABLE S1. Nuclear T_1 (in seconds) at 9.2 T for a range of TEMPOL concentrations. These values were used to calculate the relaxivities in Fig. 11 of the main text. The reported temperatures of the samples were deduced as described in Ref. 5.

| TEMPOL | acetone | | | DMSO | |
|---------|---------|--------|--------|--------|--------|
| | 29.1°C | 31.9°C | 41.9°C | 21.9°C | 39.0°C |
| 0 mM | 2.751 | 2.818 | 3.091 | 2.539 | 3.446 |
| 5 mM | 2.039 | - | - | 0.783 | 1.093 |
| 20 mM | 1.046 | - | - | 0.257 | 0.379 |
| 40 mM | 0.401 | - | - | 0.134 | 0.192 |
| 60 mM | - | 0.427 | 0.484 | 0.100 | 0.141 |
| 100 mM | 0.193 | 0.209 | 0.236 | 0.056 | 0.079 |
| 150 mM | - | 0.168 | 0.188 | 0.038 | 0.054 |
| 200 mM | 0.1072 | - | - | 0.027 | 0.040 |
| 500 mM | - | 0.058 | 0.065 | 0.014 | 0.020 |
| 1000 mM | - | 0.014 | 0.015 | 0.007 | 0.010 |

TABLE S2. Information about the MD simulations of pure solvents or liquids containing 1 TEMPOL.

| | $\rho/\text{kg m}^{-3}$ | L/nm | $T_{\text{pure}}/\text{ns}$ | T_{low}/ns |
|------------|-------------------------|---------------|-----------------------------|----------------------------|
| acetone | 778 | 6.9811 | 1+6 | 1+10 |
| DMSO/DMSO* | 1085 | 6.8964 | 1+6 | 1+20 |

fully choosing the friction coefficients of the Langevin thermostat that maintains the temperature of the MD simulations, we ensured that the diffusion constants of the simulated solutions match the experimental values at 35°C.^{13,14} To this end, several constant volume (NVT) simulations were performed for 7 ns with different values of the friction coefficient, γ . The first 1 ns was not analyzed. Diffusion coefficients were estimated from the slope of the mean square displacement in the time interval 400–500 ps. Displacements in the three Cartesian directions were analyzed separately and used to calculate an average and standard deviation. The values of γ for which the average diffusion coefficient was within one standard deviation of the experimental target was selected for the subsequent simulations. These are reported in Table 1 of the main text. The small numerical values of the employed friction (Table 1, main text) indicate that the thermostat does not introduce artificial fast (\sim ps) dynamics.

For simulations with TEMPOL at infinite dilution, 1 TEMPOL molecule was placed into the pure solvent boxes. Four acetone and three DMSO molecules that overlapped with the TEMPOL were removed from the boxes. Constant volume simulations were performed for 11 ns for acetone and 21 ns for DMSO. The first 1 ns was not analyzed (last column of Table S2). Atomic coordinates were saved every 0.2 ps, which is several times less than the electron Larmor frequency at 260 GHz.

For the simulations with high (1M) TEMPOL concentration, 176 TEMPOL molecules were placed into the pure acetone box and 177 TEMPOL molecules were placed into the pure DMSO box. After removing the

TABLE S3. Information about the MD simulations with 1 M TEMPOL.

| | # TEMPOL+solvent | L/nm | $\rho/\text{kg m}^{-3}$ | $T_{\text{high}}/\text{ns}$ |
|---------|------------------|---------------|-------------------------|-----------------------------|
| acetone | 176+2048 | 6.6737 | 801 | 5 |
| DMSO | 177+2040 | 6.6689 | 1063 | 10 |
| DMSO* | 177+2040 | 6.7127 | 1042 | 10 |

overlapping solvent molecules, 2048 acetone and 2040 DMSO molecules remained (Table S3). Since experimental density information about the 1 M TEMPOL solutions was not available, constant pressure (NPT) simulations were performed for 10 ns to estimate the volume. The average volume of the simulation box over this period was calculated. The box sizes were then fixed by keeping the side lengths at the values given in the third column of Table S3, which imply the densities reported in the fourth column of the same table. After that, constant volume (NVT) simulations were performed for a duration of T_{high} ns.

B. Densities

In order to validate the densities obtained by the computational procedure outlined at the end of the previous paragraph we conducted additional experiments and measured the densities of pure DMSO and of 1 M TEMPOL in DMSO. The density of pure DMSO at 20°C was found to be 1116.64 kg/m³. Given that the literature value is 1100.53 kg/m³,¹⁵ our density measurements are seen to be reliable to within 1.5%.

The density of 1 M TEMPOL in DMSO that we measured at 20°C was 1103.18 kg/m³, which is about 1% lower than our measurement for pure DMSO. Assuming that this relation applies also at 35°C, where we have not performed density measurements, in the MD simulations at this temperature we should observe similar densities for pure DMSO and 1 M TEMPOL in DMSO.

To check this, we simulated pure DMSO (and DMSO*) at 35°C under constant pressure and calculated the average volume. The densities deduced from these simulations are 1078.5 kg/m³ for DMSO and 1049.9 kg/m³ for DMSO*. In line with our expectation, both of these values are slightly larger than the densities of the simulated DMSO-TEMPOL solutions reported in Table S3. Thus, the computationally deduced densities of 1 M TEMPOL in DMSO and in DMSO* are reasonable.

Coming back to the simulations of pure DMSO with the two alternative models, DMSO and DMSO*, we note that the MD densities (1078.5 kg/m³ for DMSO and 1049.9 kg/m³ for DMSO*) differ from the experimental value at 35°C (1085.24 kg/m³)¹⁶ by less than 1% and slightly more than 3%, respectively. Clearly, while the modified model DMSO* improves the dielectric relaxation properties of the solvent, it has an adverse effect on the liquid density. This observation is a nice illustration

of our claim that the proper development of force-field parameters requires a separate full-blown effort.

C. Dielectric response

The frequency response of the dielectric permittivity is related to the collective electric dipole moment of the entire simulation box with N molecules, expressed as

$$\mathbf{M}(t) = \sum_{a=1}^N \mu_a, \quad (\text{S2})$$

where the vector μ_a is the electric dipole moment of molecule a . Let us denote the time correlation functions (TCFs) of the Cartesian components of $\mathbf{M}(t)$ as

$$\Phi_{ij}(t) = \langle M_i(\tau)M_j(\tau+t) \rangle_{\tau}, \quad (\text{S3})$$

where the angle brackets denote ensemble average and the subscript denotes an additional average over the time variable τ . For a rotationally isotropic system we should have $\Phi_{ij}(t) = \delta_{ij}\Phi(t)$, where δ_{ij} is Kronecker's delta. Thus, $\Phi(t)$ can be estimated by averaging $\Phi_{xx}(t)$, $\Phi_{yy}(t)$ and $\Phi_{zz}(t)$. The standard deviation of the three independent estimates can also be obtained.

The frequency-dependent dielectric constant $\epsilon(\omega)$ is related to the TCF $\Phi(t)$ through the relation^{17,18}

$$\epsilon(\omega) = 1 + \frac{1}{Vk_B T \epsilon_0} \mathcal{L}[-\dot{\Phi}(t)](\omega), \quad (\text{S4})$$

where V is the volume of the simulation box, $k_B T$ is the thermal energy at temperature T , $\epsilon_0 = 8.85 \times 10^{-12}$ F/m is the permittivity of vacuum, $\dot{\Phi} = d\Phi/dt$, and $\mathcal{L}[g]$ is the Fourier-Laplace (or one-sided Fourier) transform of g ,

$$\mathcal{L}[g(t)](\omega) = \int_0^{\infty} g(t)e^{-i\omega t} dt. \quad (\text{S5})$$

We first fit the TCF $\Phi(t)$ obtained from the simulations with a sum of two or three exponential decays,

$$\Phi(t) = \sum_i a_i e^{-t/\tau_i}, \quad (\text{S6})$$

over the range 0–1 ns. The amplitudes, a_i (Debye squared), and relaxation time scales, τ_i (ps), are given in Table S4 (acetone), Table S5 (DMSO) and Table S6 (DMSO*) for the simulations of pure solvent, dilute (1 TEMPOL) and concentrated (1 M TEMPOL) solutions. From the tables, the dominating timescales are seen to be ~ 3 ps for acetone, 20–25 ps for DMSO, and 15–20 ps for DMSO*. The values vary with the concentration of TEMPOL.

Using the multiexponential fit, we obtain the one-sided Fourier transform

$$\mathcal{L}[-\dot{\Phi}](\omega) = \sum_i \frac{a_i}{1 + \tau_i^2 \omega^2} - i\omega \sum_i \frac{a_i \tau_i}{1 + \tau_i^2 \omega^2}. \quad (\text{S7})$$

TABLE S4. Multiexponential fitting parameters for acetone.

| Pure | | 1 TEMPOL | | 1 M TEMPOL | |
|-----------|--------------------|-----------|--------------------|------------|--------------------|
| a_i/D^2 | τ_i/ps | a_i/D^2 | τ_i/ps | a_i/D^2 | τ_i/ps |
| 1273 | 0.985 | 332 | 0.558 | 582 | 0.260 |
| 22260 | 3.20 | 23167 | 3.07 | 12709 | 2.87 |
| | | | | 3869 | 17.2 |

TABLE S5. Multiexponential fitting parameters for DMSO.

| Pure | | 1 TEMPOL | | 1 M TEMPOL | |
|-----------|--------------------|-----------|--------------------|------------|--------------------|
| a_i/D^2 | τ_i/ps | a_i/D^2 | τ_i/ps | a_i/D^2 | τ_i/ps |
| 2113 | 0.398 | 1505 | 0.265 | 2292 | 0.480 |
| 4587 | 5.46 | 6683 | 4.83 | 40176 | 22.1 |
| 54545 | 20.8 | 66415 | 24.4 | 6707 | 394 |

Thus, for the real and imaginary parts of

$$\epsilon(\omega) = \epsilon'(\omega) - i\epsilon''(\omega) \quad (\text{S8})$$

we find

$$\epsilon'(\omega) = 1 + \frac{1}{Vk_B T \epsilon_0} \sum_i \frac{a_i}{1 + \tau_i^2 \omega^2} \quad (\text{S9})$$

and

$$\epsilon''(\omega) = \frac{\omega}{Vk_B T \epsilon_0} \sum_i \frac{a_i \tau_i}{1 + \tau_i^2 \omega^2}. \quad (\text{S10})$$

Note that the static value of ϵ (reported in Table 1 of main text), which corresponds to $\omega = 0$, is purely real and can be obtained from the initial value of the TCF through the relation:

$$\epsilon = \epsilon'(0) = 1 + \frac{1}{3Vk_B T \epsilon_0} \langle \mathbf{M}(\tau) \cdot \mathbf{M}(\tau) \rangle_\tau. \quad (\text{S11})$$

For a mixture, one can calculate the self- and cross-contributions of the separate components to the TCF and, thus, to $\epsilon(\omega)$. Denoting the electric dipole moments of all the solvent molecules in the simulation box by \mathbf{M}_S and all the TEMPOL molecules by \mathbf{M}_T , we have

$$\Phi(t) = \Phi_{SS}(t) + \Phi_{ST}(t) + \Phi_{TT}(t), \quad (\text{S12})$$

where

$$\Phi_{SS}(t) = \frac{1}{3} \langle \mathbf{M}_S(\tau) \cdot \mathbf{M}_S(t + \tau) \rangle_\tau, \quad (\text{S13})$$

TABLE S6. Multiexponential fitting parameters for DMSO*.

| Pure | | 1 TEMPOL | | 1 M TEMPOL | |
|-----------|--------------------|-----------|--------------------|------------|--------------------|
| a_i/D^2 | τ_i/ps | a_i/D^2 | τ_i/ps | a_i/D^2 | τ_i/ps |
| 3146 | 0.859 | 947 | 0.146 | 2358 | 0.790 |
| 56644 | 19.4 | 57986 | 15.9 | 35888 | 17.0 |
| 1456 | 64.6 | 1027 | 49.1 | 1315 | 220 |

$$\Phi_{TT}(t) = \frac{1}{3} \langle \mathbf{M}_T(\tau) \cdot \mathbf{M}_T(t + \tau) \rangle_\tau \quad (\text{S14})$$

and

$$\Phi_{ST}(t) = \frac{2}{3} \langle \mathbf{M}_S(\tau) \cdot \mathbf{M}_T(t + \tau) \rangle_\tau. \quad (\text{S15})$$

Using each of these additive components in (S4) allows us to write

$$\epsilon(\omega) = \epsilon_{SS}(\omega) + \epsilon_{ST}(\omega) + \epsilon_{TT}(\omega), \quad (\text{S16})$$

as claimed in the main text. In practice, separate multiexponential fits were performed for each of the self- and cross-TCF and used in (S10).

D. Magnetic dipole-dipole coupling

Magnetic dipole-dipole TCFs can be calculated from the coordinates of the spins at two instances τ and $\tau + t$ as follows:

$$C_m(t) = \langle F_m^*(\mathbf{r}, \tau) F_m(\mathbf{r}, \tau + t) \rangle_\tau. \quad (\text{S17})$$

Here,

$$F_m(\mathbf{r}, t) = \frac{Y_2^m(\theta(t), \phi(t))}{r(t)^3}, \quad (\text{S18})$$

Y_2^m 's are the rank-2 spherical harmonics, and (r, θ, ϕ) are the spherical coordinates of the vector between the spins, \mathbf{r} . In a rotationally isotropic environment, the TCFs are expected to be independent of m . Thus another averaging is performed over $m = -1, 0, 1$ to calculate an m -independent TCF, $C(t)$. The dipolar spectral density function (SDF) is the real part of the Fourier-Laplace transform of the TCF:

$$J(\omega) = \text{Re}\{\mathcal{L}[C(t)](\omega)\}. \quad (\text{S19})$$

The calculation and normalization of near-near and near-far TCFs was performed as described elsewhere.² Calculated correlation lengths were 1 ns for acetone and 2 ns for DMSO and DMSO* due to the slower decay rate of the DMSO correlations (*cf.* Fig. 7 in main text). The time resolution of the correlation functions was $\Delta t = 0.2$ ps, which is the frequency with which the coordinates were recorded. This resolution in time limits the frequency bandwidth of the numerical Fourier transform of the TCF to $F = 1/\Delta t = 5000$ GHz. The total duration of the TCF, on the other hand, sets a limit on the frequency resolution. For acetone we had $\Delta f = 0.5$ GHz, whereas for DMSO and DMSO* the resolution was two times higher, $\Delta f = 0.25$ GHz, as reflected by the lowest frequency points in Fig. 8 of the main text.

The near-near TCFs were fit to a sum of decaying exponential functions in order to calculate the SDFs through analytical Fourier transforms, since for

$$C_{NN}(t) = \sum_{i=1}^4 a_i e^{-t/\tau_i} \quad (\text{S20})$$

we have

$$J_{\text{NN}}(\omega) = \sum_{i=1}^4 \frac{a_i \tau_i}{1 + \omega^2 \tau_i^2}. \quad (\text{S21})$$

The intensities and relaxation time scales of the fits are shown in Tables S7 and S8.

TABLE S7. Near-near TCF fitting parameters for liquids with 1 TEMPOL.

| Acetone | | DMSO | | DMSO* | |
|-------------------|--------------------|-------------------|--------------------|-------------------|--------------------|
| a_i/nm^3 | τ_i/ps | a_i/nm^3 | τ_i/ps | a_i/nm^3 | τ_i/ps |
| 2.841 | 0.242 | 2.801 | 0.414 | 2.876 | 0.395 |
| 2.768 | 1.71 | 3.237 | 5.99 | 3.313 | 5.62 |
| 2.601 | 9.29 | 2.768 | 50.9 | 2.705 | 46.1 |
| 0.583 | 36.8 | 0.469 | 241 | 0.730 | 204 |

TABLE S8. Near-near TCF fitting parameters for solutions with 1 M TEMPOL.

| Acetone | | DMSO | | DMSO* | |
|-------------------|--------------------|-------------------|--------------------|-------------------|--------------------|
| a_i/nm^3 | τ_i/ps | a_i/nm^3 | τ_i/ps | a_i/nm^3 | τ_i/ps |
| 3.087 | 0.249 | 2.827 | 0.419 | 2.976 | 0.392 |
| 2.738 | 1.86 | 2.994 | 6.45 | 3.225 | 5.25 |
| 2.642 | 10.8 | 2.434 | 55.4 | 2.540 | 42.2 |
| 0.658 | 44.0 | 0.799 | 243 | 0.735 | 182 |

The near-near SDFs calculated by assuming that the spins are at the molecular centers of mass (COM) were fit with the finite-size version of the HSCS model. Note that these are only used in the calculation of the finite-size correction $\Delta_{\text{NN}}^{\text{fs}}$ in Eq. (5) of the main text. The fitting parameters b and D are given in Table 4 of the main text (rows labeled J_{NN}).

Although not required by our methodology, one can envision fitting the actual (spins at their correct positions away from the molecular centers) near-near SDFs with the finite-size version of the HSCS model. Such fits are depicted in Fig. S5. The fitting parameters are $b = 0.38$ nm, $D = 5.95$ nm²/ns for acetone, and $b = 0.40$ nm, $D = 1.03$ nm²/ns for DMSO. Clearly, they are different from the values reported in the last three rows of Table 4 of the main text. The fits in Fig. S5, however, seem to be comparable in quality to the ones for the near-near SDFs calculated by assuming that the spins are at the molecular COM and shown in Fig. 8a of the main text.

If the finite-size version of the HSCS model fits the actual near-near SDFs, why do we use multiexponential fits to the near-near TCFs [*cf.* Eq. (S20)]? Even more importantly, how can a model assuming centered spins fit the SDFs of off-centered spins? To investigate this point, the plots in Fig. 8a and Fig. S5 are reproduced in Fig. S6 with logarithmic scales on both the vertical and horizontal axes. We observe that the near-near SDFs calculated from the MD simulations by assuming that

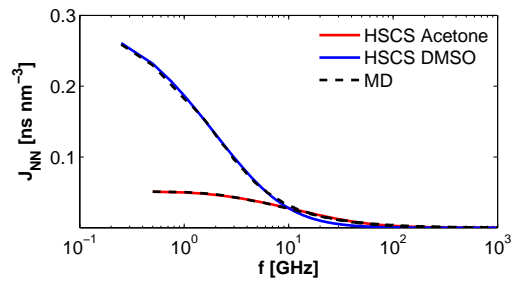


FIG. S5. Near-near SDFs calculated from the MD simulations for spins at their actual positions (dashed lines) and best fits with the finite-size HSCS model (solid lines).

the spins are at the centers of the molecules (dashed lines in Fig. S6a) agree well with the analytical model (solid lines) over the whole frequency range. In contrast, the near-near SDFs calculated from the MD simulations by using the actual positions of the spins (dashed lines in Fig. S6b) deviate substantially from the predictions of the HSCS model at the higher frequencies shown in the figure. In Fig. S6b the slopes of the analytical lines at high frequencies are very different than the slopes of the MD lines. This confirms our expectation that at short spin-spin distances, as is the case in the near region, the HSCS model should fail to fit the actual near-near SDF. A multiexponential fit does an excellent job at fitting the MD lines in Fig. S6b (not shown).

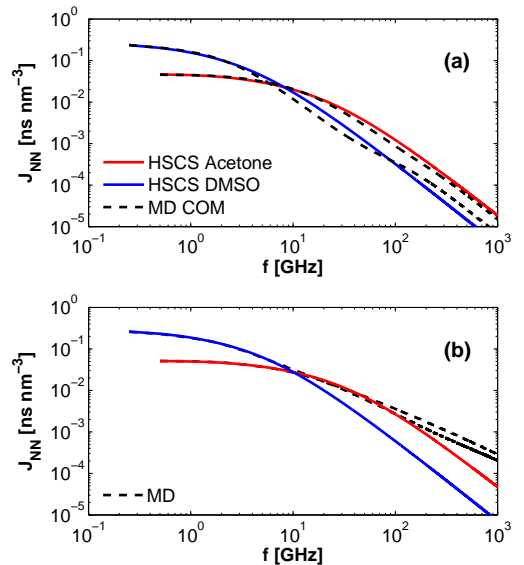


FIG. S6. (a) Same as Fig. 8a in main text with logarithmic vertical axis. (b) Same as Fig. S5 with logarithmic vertical axis.

-
- * dsezer@sabanciuniv.edu
- ¹ B. Halle, *J. Chem. Phys.* **119**, 12373 (2003).
 - ² D. Sezer, *Phys. Chem. Chem. Phys.* **15**, 526 (2013).
 - ³ Y. Ayant, E. Belorizky, J. Alizon, and J. Gallice, *J. Phys. (Paris)* **36**, 991 (1975).
 - ⁴ L.-P. Hwang and J. H. Freed, *J. Chem. Phys.* **63**, 4017 (1975).
 - ⁵ P. Neugebauer, J. G. Krummenacker, V. P. Denysenkov, C. Helmling, C. Luchinat, G. Parigi, and T. F. Prisner, *Phys. Chem. Chem. Phys.* **16**, 18781 (2014).
 - ⁶ K. Vanommeslaeghe, E. Hatcher, C. Acharya, S. Kundu, S. Zhong, J. Shim, E. Darian, O. Guvench, P. Lopes, I. Vorobyov, and A. D. Mackerell, *J. Comput. Chem.* **31**, 671 (2010).
 - ⁷ M. L. Strader and S. E. Feller, *J. Phys. Chem. A* **106**, 1074 (2002).
 - ⁸ P. Bordat, J. Sacristan, D. Reith, S. Girard, A. Glättli, and F. Müller-Plathe, *Chem. Phys. Lett.* **374**, 201 (2003).
 - ⁹ D. Sezer, J. H. Freed, and B. Roux, *J. Phys. Chem. B* **112**, 5755 (2008).
 - ¹⁰ J. C. Phillips, R. Braun, W. Wang, J. Gumbart, E. Tajkorshid, E. Villa, C. Chipot, R. D. Skeel, L. Kale, and K. Schulten, *J. Comp. Chem.* **26**, 1781 (2005).
 - ¹¹ U. Essmann, L. Perera, M. L. Berkowitz, T. Darden, H. Lee, and L. G. Pedersen, *J. Chem. Phys.* **103**, 8577 (1995).
 - ¹² S. Miyamoto and P. A. Kollman, *J. Comp. Chem.* **13**, 952 (1992).
 - ¹³ H. Ertl and F. A. L. Dullien, *AIChE Journal* **19**, 1215 (1973).
 - ¹⁴ M. Holz, S. R. Heil, and A. Sacco, *Phys. Chem. Chem. Phys.* **2**, 4740 (2000).
 - ¹⁵ N. G. Tsierkezos, A. E. Kelarakis, and M. M. Palaiologou, *J. Chem. Eng. Data* **45**, 395 (2000).
 - ¹⁶ U. R. Kapadi, S. K. Chavan, and O. S. Yemul, *J. Chem. Eng. Data* **42**, 548 (1997).
 - ¹⁷ C. J. F. Böttcher and P. Bordewijk, *Theory of Electric Polarization*, 2nd ed., Vol. II: Dielectrics in Time-Dependent Fields (Elsevier Science B. V., 1978).
 - ¹⁸ S. Gekle and R. R. Netz, *J. Chem. Phys.* **137**, 104704 (2012).